Predicting the Dynamic Viscosity of High-Concentration Antibody Solutions with a Chemically Specific Coarse-Grained Model

Tobias M. Prass,[†] Patrick Garidel,[‡] Michaela Blech,[*,¶] and Lars V. Schäfer[*,†]

†*Center for Theoretical Chemistry, Ruhr University Bochum, D-44780 Bochum, Germany*

‡ *Innovation Unit, Pharmaceutical Development Biologicals, Boehringer Ingelheim Pharma GmbH & Co. KG, D-88397 Biberach an der Riss, Germany*

¶*Innovation Unit, Analytical Development Biologicals, Boehringer Ingelheim Pharma GmbH & Co. KG, D-88397 Biberach an der Riss, Germany*

E-mail: michaela.blech@boehringer-ingelheim.com; lars.schaefer@ruhr-uni-bochum.de

Abstract

The viscosity of high-concentration protein solutions is a critical parameter in biopharmaceutical formulation development. Conventionally, the viscosity is measured and optimized in labor-intensive experimental workflows that require a lot of material. While predicting the viscosity with atomistic molecular dynamics (MD) simulations is feasible, they are computationally prohibitively expensive due to the large system sizes and the long simulation times involved. Coarse-grained MD (CG-MD) simulations significantly reduce computational demands, but evaluating their accuracy and predictive power requires rigorous validation. Here, we assess the capability of the Martini 3 CG force field to predict the viscosity of high-concentration antibody solutions. We show that a refined Martini 3 force field, with optimized protein–protein interactions, can accurately predict the elevated viscosities observed in concentrated solutions of the therapeutic monoclonal antibody (mAb) omalizumab. Furthermore, we show that our previously developed Martini 3-exc model for arginine excipients successfully captures the trend of lowering viscosity, as observed in our rheology experiments. These findings open the way to physics-based computational prediction of the properties of dense biopharmaceutical solutions via large-scale MD simulations.

Introduction

High-concentration protein solutions are central to numerous biological and pharmaceutical applications. In the context of biopharmaceuticals, high-concentration formulations are particularly desirable for subcutaneous injection, as they enable self-administration of therapeutic doses in small volumes. However, developing high-concentration formulations involves significant challenges, including issues related to protein conformational stability, particle formation, phase separation, and elevated viscosity;[1–6] for a recent review, see Manning et al.[7] The crowded macromolecular environment in these solutions can influence biomolecular structure and solvation, and the kinetics of molecular processes.[8–13]

Monoclonal antibodies (mAbs), a major class of biopharmaceuticals, are especially affected by these factors due to their large size and conformational flexibility. mAbs are widely used in the treatment of diseases ranging from cancer and multiple sclerosis to asthma and COVID-19.[14] The high therapeutic dosages required (up to 15 mg per kg body weight) and the limited volumes suitable for subcutaneous injection (up to about 3 ml)[15] necessitate mAb concentrations of 100 mg/ml or higher. Elevated viscosity in these formulations is associated with increased injection forces, tissue back-pressure, and injection pain, while protein particles can decrease drug efficacy and trigger immunogenic responses.[15,16]

Traditionally, strategies to optimize the stability and properties of biopharmaceutical solutions rely on empirical trial-and-error workflows that screen various combinations of buffers and excipients, such as salts and amino acids.[17,18] Given the high production costs of mAbs,[19] computational methods that can predict the viscosity of high-concentration formulations would be highly advantageous. Molecular dynamics (MD) simulations can, in principle, resolve the relevant molecular-level interactions underlying the properties of these systems. Our previous work demonstrated that all-atom MD simulations can correctly capture the increase in dynamic viscosity with rising mAb concentration.[20] However, the computational resources required for statistically robust results are enormous, limiting the practical application of such approaches.[20] Alternative, more easily accessible methods include colloidal

hard-sphere models[21–23] or super-coarse grained (CG) representations that model mAbs with as few as, for example, 6, 12, or 24 CG beads and omit explicit solvent.[24–27] Such computationally cheap models enable long time scale simulations of systems with a large number of mAb molecules. However, the reduced accuracy associated with the reduction of the proteins to a very coarse (sub-)domain level representation limits the predictive power of such super-CG models and necessitates careful parametrization and validation against experiments or higher-level simulations.

The molecular mechanisms governing the properties of high-concentration mAb solutions, as well as the viscosity-reducing and aggregation-mitigating effects of excipients, remain incompletely understood. Arginine, a widely used amino acid-based excipient, is known to mitigate viscosity and aggregation.[28–30] Recent atomistic MD studies have focused on on the effect of arginine on the Fab domains of mAbs, highlighting the interactions of arginine excipients with aromatic and charged amino acids.[31–33] To directly investigate excipient effects on high-concentration solutions, a computationally efficient compromise between the super-CG and atomistic representation is desired – one that balances chemical specificity and sufficient sampling capability. Such a model should combine an explicit description of protein–excipient interactions with long-timescale simulations to sample all relevant configurations, in particular, the diverse protein–protein interaction interfaces and their modulation by excipient molecules.

The Martini CG force field is a widely used approach that achieves this balance by mapping fragments of two to four heavy atoms (plus the associated hydrogens) to a single CG bead. This level of resolution retains chemical specificity of protein–excipient interactions.[34,35] The latest version, Martini 3, has improved interaction parameters compared to its predecessor Martini 2[36] and can be used for large-scale multi-protein simulations.[37–39] However, the scale of the protein–protein interactions remains a potential shortcoming of Martini 3. For example, Thomasen et al. reported that Martini 3 yields too compact structures of intrinsically disordered protein (IDP) and multidomain proteins. They suggested

to either increase the protein–water interactions or decrease the protein–protein interactions (PPIs) (by changing the well depths of the nonbonded Lennard-Jones (LJ) potentials by +10 % and -12 %, respectively).[40,41] Binder et al. improved PPIs of lysozyme and subtilisin systems by applying separate scalings of nonbonded interactions between organic and ionic bead types.[42] The Martini3-IDP force field addresses overly compact conformational ensembles of IDPs by adjusting the bonded interactions in the force field, improving agreement with experimental data.[43] Pedersen et al. and Lamprakis et al. reported unstable protein complexes with Martini 3 that were stable in all-atom simulations.[44,45] These findings suggest that the remaining inaccuracies in the model arise from factors that are more complex than a simple global over- or underestimation of protein–protein and/or protein–water interaction strength.

Dynamic (shear) viscosity can be computed from equilibrium MD simulations with a Green-Kubo (GK) formalism, which relates viscosity to the integral over the pressure autocorrelation function (ACF)[46,47]

$$\eta = \lim_{t\to\infty} \eta(t) = \frac{V}{k_B T} \lim_{t\to\infty} \int_0^t \langle P_{\alpha\beta}(t_0)\, P_{\alpha\beta}(t_0 + t)\rangle \, dt \tag{1}$$

where V is the volume of the simulation box, k_B is Boltzmann's constant, T is the temperature, and $\langle \ldots \rangle$ indicates thermal averaging. $P_{\alpha\beta}$ are the nondiagonal elements of the pressure tensor, whose ACFs are calculated by averaging over all time origins t_0. A major challenge of this method is sampling. The viscosity computed from the GK integral (eq. 1) is exact in the asymptotic (long-time) limit, whereas the timescales accessible with simulations are limited (μs up to maybe ms). Moreover, the large pressure fluctuations in the microscopic simulation systems result in slow convergence of the GK integrals. Large-scale all-atom MD simulations in explicit solvent have been used to study viscosity and diffusion in concentrated solutions of small proteins, which do not exhibit very high viscosities.[48] Our previous all-atom MD simulation study of a highly viscous mAb solution demonstrated that

the GK approach can capture the experimental trend of viscosity changes with protein concentration.[20] However, despite the huge computational resources required for achieving the multi-μs time scales in the all-atom simulations, the statistical precision of the computed viscosity predictions was limited, and only a single system could be investigated.[20] Furthermore, only small simulation systems containing four mAb molecules could be studied in our previous all-atom simulations.

In this work, we combine MD simulations and rheology experiments to assess the capability of the Martini 3 CG force field to predict the viscosity of high-concentration mAb solutions. Specifically, we address three key questions: (1) How does scaling of protein–protein interactions in Martini 3 affect viscosity predictions? (2) Can Martini 3 describe the increase in viscosity with rising mAb concentration? (3) Can the model capture the experimentally observed modulation of viscosity by arginine excipients? We use the therapeutic antibody omalizumab (Xolair®) as a model system, as its high-concentration solutions exhibit pronounced viscosity increases in the absence of excipients and substantial viscosity reduction upon addition of arginine chloride (Arg/Cl).

To facilitate MD simulations, we used F(ab')$_2$ fragments rather than full-length mAbs (Figure 1). This approach circumvents the need to model the glycosylated Fc domain of the mAb, which is a challenge because carbohydrate parameters for glycosylated amino acids are still under development and are not yet available in Martini 3.[49–51] Furthermore, the smaller system sizes enable longer simulation times and larger simulation systems. We simulated systems containing 32 omalizumab F(ab')$_2$ fragments to investigate the viscosity of the high-concentration solutions (Figure 1). We tested different PPI scalings in Martini 3, including the 12% scaling of the well-depths of the Lennard-Jones interactions between protein beads suggested by Thomasen et al. for IDPs,[40,41] and compare the resulting viscosities to experimental values. We also incorporated our previously developed arginine excipient model for Martini 3[52] to evaluate whether the refined CG model captures the viscosity difference between Na/Cl and Arg/Cl environments. Finally, we probed mAb concentrations of 150, 200,

and 250 mg/ml to investigate concentration-dependent changes in viscosity. Corresponding rheological measurements were performed for omalizumab F(ab')$_2$ at different concentrations and in different excipient environments.

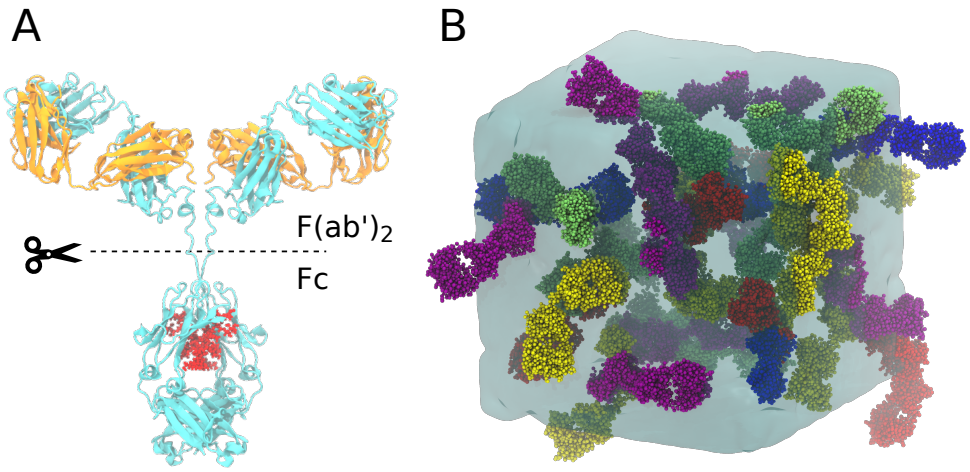

Figure 1: A) Molecular representation of full-length omalizumab. The cleavage into F(ab')$_2$ and Fc fragments is indicated by the dashed line. The heavy and light chains are shown in cyan and orange, respectively, and the glycan in the Fc domain is shown in red. B) Snapshot of one of the simulation systems containing 32 F(ab')$_2$ fragments at a concentration of 200 mg/ml.

Results and Discussion

PPI Scaling Improves Agreement with Experiment

We first analyzed simulations of F(ab')$_2$ systems at a concentration of 200 mg/ml (with 150 mM Na/Cl), using both the original Martini 3 force field parameters and a modified force field in which the protein–protein interactions were weakened by reducing the well-depths ϵ_{LJ} of the Lennard-Jones interaction potentials between protein beads. The scaling of ϵ_{LJ} was varied between 6% and 36%. For each system, five independent 5 μs MD simulations were run (25 μs in total), see Methods. The resulting Green-Kubo integrals and the final viscosity values are shown in Figure 2 and Table 1; GK integrals from the five individual repeat simulations are shown in Figure S1.

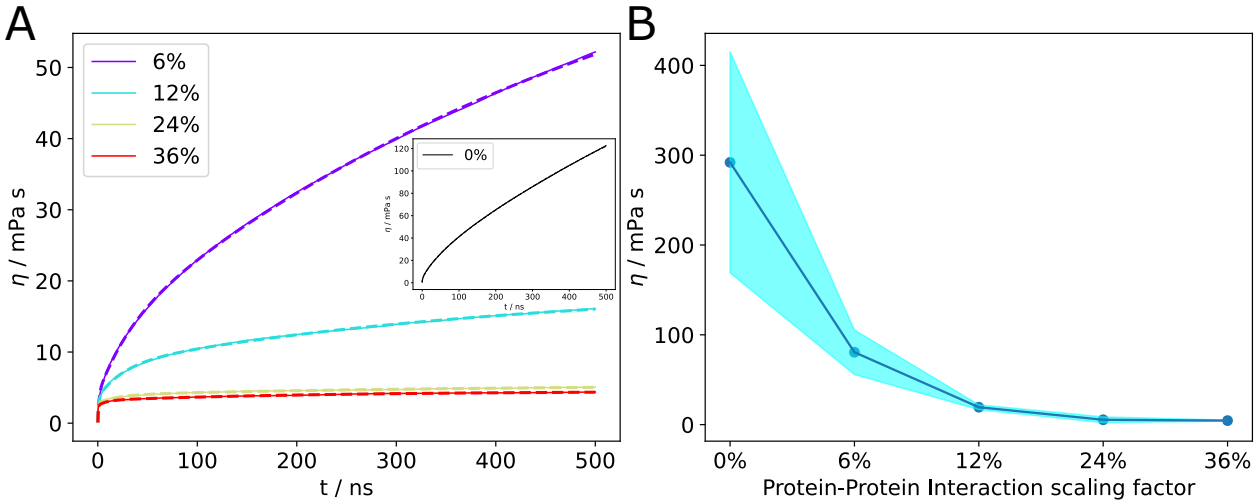

Figure 2: A) Green-Kubo integrals (solid lines) from the CG-MD simulations with the different PPI scalings. Exponential fits are shown as dashed lines. The inset in A) shows the results for the original (unscaled) Martini 3 force field. B) Dynamic viscosities obtained from the asymptotic limit of the exponential fits. The uncertainty (shaded area) represents the standard deviation of the computed values from the five individual repeat simulations.

The original Martini 3 force field yields a very high viscosity close to 300 mPa · s, with large statistical uncertainty due to the incomplete sampling of the ultraslow dynamics related to the reconfiguration of the sticky protein network in this highly viscous system. Weakening the attractive interactions between the protein CG beads by scaling the Lennard-Jones potentials strongly reduces the viscosity, with 6% and 12% PPI scalings yielding viscosity values of 80.6 and 19.4 mPa · s, respectively (Table 1). As a baseline or reference value, the viscosity of pure Martini 3 water is 0.66 mPa · s at 300 K (Figure S2).

Table 1: Dynamic viscosities from the Martini 3 simulations of the 200 mg/ml F(ab')$_2$ systems with 150 mM Na/Cl and the different PPI scalings applied.

PPI scaling	Viscosity (mPa · s)
0%	291.5 ± 123.4
6%	80.6 ± 24.8
12%	19.4 ± 2.7
24%	5.4 ± 3.2
36%	4.5 ± 0.6

To experimentally validate the viscosity values predicted by the CG-MD simulations, we measured the viscosity of omalizumab F(ab')$_2$ fragments at different concentrations (Table 2).

Our rheology measurements yielded viscosities of 12.6 and 37.1 mPa · s at the concentrations of 149 and 204 mg/ml, respectively. These values are in line with Heisler et al., who reported a viscosity of 19.3 mPa · s for a 180 mg/ml omalizumab F(ab')$_2$ solution.[53]

The discrepancy between the simulated and experimental viscosities suggests that improvements can be achieved by weakening the attractive protein–protein interactions in the Martini 3 force field. While it is possible to adjust the PPI scaling such as to quantitatively reproduce the experimental viscosity values, such an approach might be system-specific and would raise the risk of overfitting. Instead, we used the 12% scaling previously introduced by Thomasen et al.[40,41] for IDPs, accepting that the viscosities are slightly lower than experimental values (19.4 mPa · s at 200 mg/ml in the CG-MD simulation versus 37.1 mPa · s at 204 mg/ml in the rheology experiment). The primary goal of the CG-MD simulation approach is not necessarily to exactly reproduce the experimental numbers, but to predict trends, such as the effects of excipients (see below).

As a control, to exclude finite box size effects, we repeated the simulations at 200 mg/ml with a two times larger system containing 64 F(ab')$_2$ fragments, yielding a dynamic viscosity of 16.1 ± 2.2 mPa · s (Figure S3) that is consistent with the value obtained with 32 F(ab')$_2$ fragments. In addition, the effect of pH was investigated by performing additional simulations at 12% PPI scaling in which low pH conditions were mimicked by doubly protonating (i.e., positively charging) all histidine side chains in the F(ab')$_2$. The resulting viscosity (Figure S4) is statistically indistinguishable from that obtained with standard histidine protonation states (21.8 ± 3.9 versus 19.4 ± 2.7 mPa · s).

CG-MD Simulations Capture Excipient Effects

We previously developed a new model for arginine excipients in Martini 3, which also involved reparametrizing the arginine–protein interactions at the single-residue level against reference data from all-atom simulations (coined the Martini3-exc model).[52] Since the excipient arginine is known to reduce the viscosity of omalizumab solutions,[54] we used our

Table 2: Dynamic viscosities obtained from rheology measurements of different omalizumab F(ab')$_2$ concentrations in presence of 150 mM Na/Cl or 150 mM Arg/Cl (pH 6.5, 10 mM histidine buffer).

Excipient conditions	F(ab')$_2$ concentration (mg/ml)	Viscosity (mPa · s)
150 mM Na/Cl	13	1.9 ± 0.2
	56	1.7 ± 0.4
	103	3.4 ± 0.1
	149	12.6 ± 0.3
	204	37.1 ± 3.5
	240	74.2 ± 2.1
150 mM Arg/Cl	9	1.2 ± 0.3
	48	1.3 ± 0.3
	98	2.6 ± 0.1
	152	7.9 ± 0.3
	196	11.9 ± 1.2
	245	26.7 ± 1.9

arginine excipient model to compare the viscosities between 150 mM Na/Cl and 150 mM Arg/Cl F(ab')$_2$ systems, thus testing the transferability and predictive capacity of the CG-MD approach. The viscosity data from the 150 mM Arg/Cl simulations are presented in Figure 3 and Table 3; the GK integrals of the five individual simulations are shown in Figure S5.

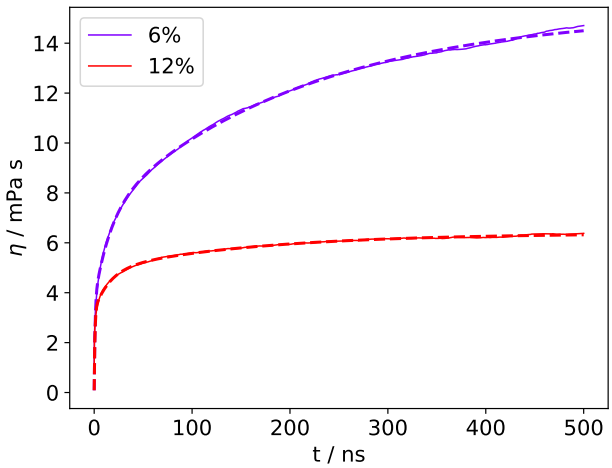

Figure 3: GK integrals (solid lines) and fits (dashed lines) from the CG-MD simulations with 150 mM Arg/Cl and PPI scalings of 6% and 12%.

In the presence of 150 mM Arg/Cl, the viscosity of the 200 mg/ml omalizumab F(ab')$_2$

Table 3: Dynamic viscosities from the CG-MD simulations of the F(ab')$_2$ at 200 mg/ml in 150 mM Arg/Cl using 6% or 12% PPI scaling. Statistical uncertainties were estimated from the standard deviations of the five independent repeat simulations run for each system.

PPI scaling	Viscosity (mPa · s)
6%	15.3 ± 3.2
12%	6.4 ± 0.5

system is reduced compared to 150 mM Na/Cl, by factors of approximately 5 and 3 with 6% and 12% PPI scaling, respectively (Tables 1 and 3). The observed viscosity reduction by a factor of about 3 at a concentration of 200 mg/ml agrees with the experimental observations (Table 2). In line with these findings, for full-length omalizumab, Tsumura et al. reported that Arg/Cl lowers viscosity by a factor of 2 to 3 compared to Na/Cl,[54] consistent with our results for the F(ab')$_2$ fragment. It is encouraging that this trend is captured in the CG-MD simulations.

The GK integrals from the simulations at the F(ab')$_2$ concentrations of 150, 200, and 250 mg/ml with 12% PPI scaling are shown in Figure 4, and the viscosity values are listed in Table 4 (the respective GK curves of the five individual simulations are plotted in Figure S6). For a comprehensive overview, Figure 5 shows the viscosity values from the simulations, the rheology experiments, and their fit to the Ross-Minton equation[55]

$$\eta = \eta_0 \exp\left[\frac{[\eta]\,\rho}{1-(k/v)\,[\eta]\,\rho}\right] \tag{2}$$

where η_0 is the dynamic viscosity of the buffer solution, $[\eta]$ is the intrinsic viscosity of the solute, c is the mass concentration, k is a crowding factor and v is a parameter that depends on the shape of the solute molecule.

Figure 5 shows the expected sharp increase in viscosity with increasing concentration, as predicted by Eq. 2. The viscosities from the CG-MD simulations with 12% PPI scaling are slightly lower than the experimental values, as discussed above. Interestingly, with 6% PPI scaling, the viscosity predicted from the simulation with Arg/Cl lies within the uncertainty of the experimental data whereas the viscosity with 150 mM Na/Cl is overestimated (red

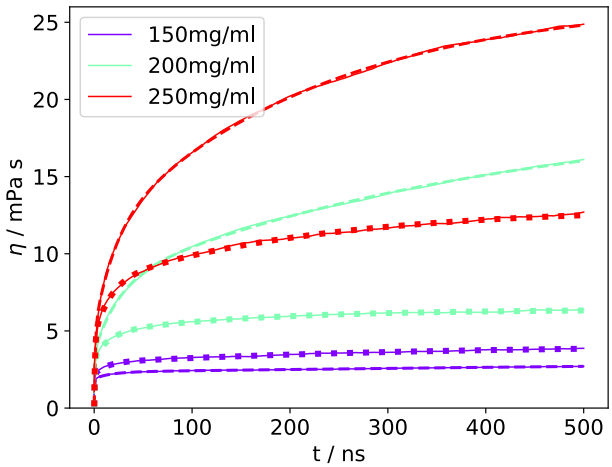

Figure 4: GK integrals from the CG-MD simulations at different F(ab')$_2$ concentrations. The solid lines depict the average GK curves (averaged over five individual simulations), and the dashed and dotted lines show the fits of the GK curves for the systems with Na/Cl and Arg/Cl, respectively

data points in Figure 5). These findings highlight remaining challenges in the optimization of the Martini 3-exc force field, likely requiring more fine-tuned adjustments than global scaling of the protein–protein interactions.

Table 4: Dynamic viscosity computed from the CG-MD simulations at different F(ab')$_2$ concentrations and excipient environments.

	Viscosity (mPa · s)	
F(ab')$_2$ concentration (mg/ml)	150 mM Na/Cl	150 mM Arg/Cl
150	3.5 ± 0.1	4.1 ± 1.9
200	19.4 ± 2.7	6.4 ± 0.5
250	26.5 ± 4.1	13.0 ± 6.3

Taken together, the results underline the suitability of the refined Martini 3-exc force field for studying high-concentration antibody solutions and predicting excipient effects, at least at a semi-quantitative level. Due to the statistical uncertainty inherently associated with the viscosity computations, small viscosity differences may not be resolvable by the approach. However, more prominent differences – such as those between Na/Cl and Arg/Cl – can be predicted by the CG-MD simulations, which is promising for formulation design.

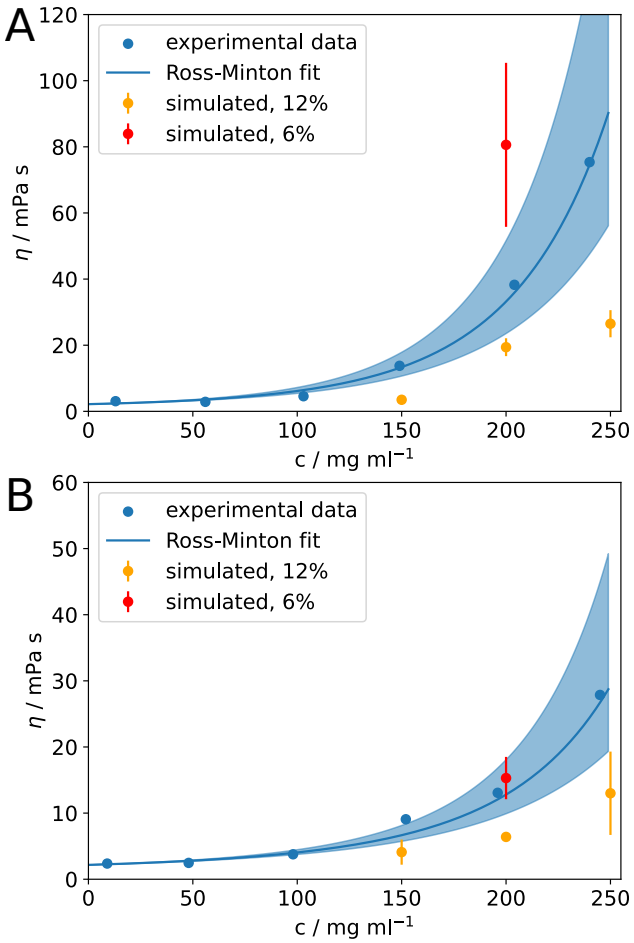

Figure 5: Comparison of dynamic viscosities from rheology experiments and CG-MD simulations. A) and B) show the data for 150 mM Na/Cl and 150 mM Arg/Cl, respectively (note different y-axis scales). Experimental data were fitted with the Ross-Minton equation (Eq. 2). The light blue shaded areas depict an estimated range resulting from an uncertainty in the experimental concentrations of ±10%.

Conclusions

This proof-of-principle study demonstrates the feasibility of using coarse-grained MD simulations with the refined Martini 3-exc force field to investigate high-concentration antibody solutions. Our results indicate that the PPI scaling originally introduced by Thomasen et al. for IDPs[40,41] is also applicable to describe the effective strength of protein–protein interactions in the dynamic protein networks underlying the high viscosity of mAb solutions. The simulations correctly reproduce the trends of increasing viscosity with rising protein concentration and the viscosity-reducing effect of arginine excipients. However, with 12% PPI

scaling, the absolute viscosity values are slightly underestimated. Rather than aiming for fully quantitative agreement of the viscosity values, the CG-MD approach introduced here enables rapid exploration of qualitative trends, and it can provide molecular-level insight into the mechanisms underlying experimental observations. Importantly, the viscosities from the simulations with different excipient environments (150 mM Na/Cl versus 150 mM Arg/Cl) are sensitive to the different nature of the ions, supporting the utility of the CG-MD approach for predicting the effects of different solvation or excipient conditions.

Some limitations remain. In the low-viscosity regime, small differences between different solvation conditions cannot be reliably resolved. In the high-viscosity regime, statistical uncertainties increase and extended simulation times (sampling) are required to observe trends with statistical significance, which can be computationally demanding even at the coarse-grained level.

Future work could extend this approach to a broader range of proteins and excipients to further validate and generalize the findings. CG-MD simulations have the potential to elucidate the molecular mechanisms underlying viscosity modulation by various formulation factors. From a practitioner's perspective, expanding the library of well-parametrized excipients and additives would facilitate the rapid implementation of the CG-MD methodology, possibly enabling more efficient pre-screening of formulation parameters in biopharmaceutical development. Beyond biopharmaceuticals, the CG-MD approach presented here may also have implications for molecular dynamics simulations of realistic models of the cell cytoplasm[56] or even entire minimal cells.[57]

Methods

MD Simulations

The atomic coordinates of the omalizumab Fab domain were obtained from the protein data bank (PDB: 2XA8).[58] The structural model of the omalizumab F(ab')$_2$ was generated using

MODELLER,[59,60] with the equilibrated trastuzumab structure from Brandt et al.[61] serving as a template. The 2XA8 structure was superimposed onto both Fab parts of the template, and the heavy chain was extended using the template structure (hinge and Fc domain). Afterwards, the full-length mAb was cleaved after H-C232, i.e., after the second disulfide bridge in the hinge region. The Martinize2 script[62] was used to convert the atomic coordinates to a coarse-grained Martini 3 representation and to generate a force field topology, including the disulfide bridges. The side chain corrections of Herzog et al.[63] were applied. Furthermore, the OLIVES[44] model was applied to the F(ab')$_2$ structures, with the recommended settings. OLIVES potentials between the two separate Fab domains of the F(ab')$_2$ dimer were removed except for the ones in the hinge region. For the CG-MD simulations, cubic simulation boxes containing 32 F(ab')$_2$ molecules were set up with protein concentrations of 150, 200, and 250 mg/ml. 150 mM Na/Cl or 150 mM Arg/Cl were added to each simulation box (2904, 2178, or 1742 of each ion species, respectively). The total number of CG beads in the 150, 200, and 250 mg/ml systems were approximately 320.000, 250.000, and 210.000, respectively. Additional control simulations at 200 mg/ml were performed with a twofold larger system containing 64 F(ab')$_2$ molecules (approximately 500.000 CG particles). For every combination (mAb and ion concentration), five independent starting configurations were generated by different random (but no clashes) initial placement of the F(ab')$_2$ molecules in the simulation boxes. The final production simulations were 5 μs long, yielding a total sampling time of 25 μs for every system.

MD simulations were performed with the GROMACS simulation package (version 2021.1)[64] using the Martini 3 force field.[37] To adjust the PPIs, all interactions between protein beads were scaled by reducing the well-depth ϵ of the Lennard-Jones (LJ) 6,12 potential (that is, making the LJ interactions less attractive) by 6%, 12%, 24%, or 36%. The simulation systems were energy minimized and afterwards equilibrated for 50 ns in the isobaric-isothermal ensemble with position restraints on the proteins at a constant temperature of 300 K and constant pressure of 1 bar, using the velocity rescaling thermostat with a stochastic term[65]

and the stochastic cell rescaling barostat,[66] respectively. The recommended "new-rf"[67] simulation settings were used with 20 fs time steps and reaction field electrostatics. Additionally, the recommended neighbor list settings by Kim et al. for simulations with Martini were applied.[68]

Viscosity Computation

For computing the dynamic viscosities from the MD simulations, we followed the approach described in detail in our previous work.[20] and computed the dynamic viscosity from the Green-Kubo (GK) integral (Eq. 1). In addition to the nondiagonal elements P_{xy}, P_{yz}, and P_{xz}, we used the following combinations of diagonal elements, $(P_{xx} - P_{yy})/2$, $(P_{xx} - P_{zz})/2$, and $(P_{yy} - P_{zz})/2$, to improve statistics.[69,70] The pressure-pressure ACFs were computed up to a maximum lag time of 500 ns (10% of the trajectory length) and averaged over all five independent 5 μs simulations. The resulting GK integrals were fitted with a triexponential function

$$\eta(t) = B \cdot \alpha \cdot \tau_1 \left(1 - e^{-t/\tau_1}\right) + B \cdot \beta \cdot \tau_2 \left(1 - e^{-t/\tau_2}\right) + B \cdot (1 - \alpha - \beta) \cdot \tau_3 \left(1 - e^{-t/\tau_3}\right) \quad (3)$$

with fitting parameters $B > 0$, $\alpha, \beta < 1$, and $\tau_{1,2,3} > 0$. The GK integrals were fitted with equation 3 up to a maximum lag time of 500 ns. As previously described,[20] the data were non-uniformly weighted in the fit (according to the standard deviation), so that the statistically more precise data at shorter lag times contribute stronger than noisy data at long lag times. The viscosity was determined from the asymptotic limit ($t \to \infty$) of the analytical fit function. The code used for these calculations is available on GitHub (`https://github.com/MolSimGroup/gmx_gk_autocorr/`).

mAb and F(ab')$_2$ Production, Purification and Formulation

The omalizumab monoclonal antibody (mAb) used in this study was supplied by Boehringer Ingelheim Pharma GmbH & Co KG (Biberach/Riss, Germany). Omalizumab, an IgG1 isotype with an approximate molecular weight of 150 kDa, was produced via mammalian cell culture in Chinese Hamster Ovary (CHO) suspension-adapted cells and purified as described previously.[20] Purification involved affinity, ion-exchange, and size-exclusion chromatography, with final formulation into 10 mM histidine buffer pH 6.5 via preparative size-exclusion chromatography.

For F(ab')$_2$ fragment generation, omalizumab was enzymatically cleaved using FabRICATOR™ (Genovis, Kävlinge, Sweden) following the manufacturer's protocol with modifications for large-scale processing. The digested sample was diluted in PBS and subjected to preparative Protein A affinity chromatography (Thermo Scientific), isolating F(ab')$_2$ in the flow-through and neutralizing with Tris buffer pH 8. The F(ab')$_2$ fragment was further polished and formulated in 10 mM histidine buffer pH 6.5 using size-exclusion chromatography. Purity and identity of omalizumab mAb and F(ab')$_2$ were confirmed by size-exclusion chromatography, non-reduced capillary gel electrophoresis, and liquid chromatography-mass spectrometry (LC-MS).

F(ab')$_2$ were concentrated to 100 mg/mL in 10 mM histidine buffer pH 6.5. Aliquots were spiked with sodium chloride (Na/Cl) or arginine hydrochloride (Arg/HCl) to prepare the following formulations: (i) 10 mM histidine pH 6.5 (non-spiked), (ii) 10 mM histidine + 150 mM NaCl pH 6.5, and (iii) 10 mM histidine + 150 mM Arg/HCl pH 6.5 with pH adjustments with concentrated base or acid as required. Samples were concentrated to 250 mg/mL or the maximum achievable concentration and subsequently diluted to 200, 150, 100, 50, and 10 mg/mL in the respective formulation buffers (i, or ii, or iii). Protein concentrations were verified using variable pathlength slope spectroscopy (SoloVPE; C Technologies Inc., New Jersey, USA), and the measured concentrations were used for rheological characterization.

Rheology Experiments

Dynamic viscosity measurements were conducted at 20 °C using a RheoSense VROC Initium One Plus rheometer (San Ramon, CA, USA) equipped with a B05 chip. A 40 μl sample volume was loaded into deactivated clear glass HPLC vials (Waters). The viscosity was evaluated across a shear rate range of 250 s^{-1} to 2000 s^{-1}, with measurements recorded at 250 s^{-1}, 500 s^{-1}, 1000 s^{-1}, 1500 s^{-1}, and 2000 s^{-1}. Data were analyzed for non-Newtonian behavior (e.g., shear thinning) or potential interfacial interaction artifacts. Dynamic viscosity was measured at a fixed shear rate of 1000 s^{-1} in six replicates per sample at 20 °C, and the mean values were reported. System suitability testing (SST) was performed using a medical-grade viscosity standard from Paragon Scientific (ISO 17025 and 17034 certified), with a reported dynamic viscosity of 9.994 mPa·s and a density of 1.1567 g/ml at 25 °C.

Supporting Information Available

Green-Kubo plots of the 200 mg/ml simulations with Na/Cl at different PPI scalings; Green-Kubo plots of the 200 mg/ml simulations with His protonation corresponding to low pH conditions; Green-Kubo plot of the 200 mg/ml simulations with 64 $F(ab')_2$; Green-Kubo plots of the 200 mg/ml simulations with Arg/Cl; Green-Kubo plots of the simulations at different mAb concentrations.

Acknowledgement

This work was supported by Boehringer Ingelheim Pharma GmbH & Co. KG and by Deutsche Forschungsgemeinschaft (DFG) under Germany's Excellence Strategy - EXC 2033 - 390677874 - RESOLV. We thank Kresten Lindorff-Larsen for useful discussions and for hosting T.P. during his internship at the University of Copenhagen.

References

(1) Frokjaer, S.; Otzen, D. E. Protein drug stability: A formulation challenge. *Nat. Rev. Drug Discov.* **2005**, *4*, 298–306.

(2) Garidel, P.; Kuhn, A. B.; Schäfer, L. V.; Karow-Zwick, A. R.; Blech, M. High-Concentration Protein Formulations: How High is High? *Eur. J. Pharm. Biopharm.* **2017**, *119*, 353–360.

(3) Éva Kollár; Balázs, B.; Tari, T.; Siró, I. Development challenges of high concentration monoclonal antibody formulations. *Drug Discov. Today Technol.* **2020**, *37*, 31–40.

(4) Woldeyes, M. A.; Qi, W.; Razinkov, V. I.; Furst, E. M.; Roberts, C. J. How well do low- and high-concentration protein interactions predict solution viscosities of monoclonal antibodies? *J. Pharm. Sci.* **2019**, *108*, 142–154.

(5) Whitaker, N.; Xiong, J.; Pace, S. E.; Kumar, V.; Middaugh, C. R.; Joshi, S. B.; Volkin, D. B. A Formulation Development Approach to Identify and Select Stable Ultra–High-Concentration Monoclonal Antibody Formulations With Reduced Viscosities. *J. Pharm. Sci.* **2017**, *106*, 3230–3241.

(6) Bauer, K. C.; Suhm, S.; Wöll, A. K.; Hubbuch, J. Impact of additives on the formation of protein aggregates and viscosity in concentrated protein solutions. *Int. J. Pharm.* **2017**, *516*, 82–90.

(7) Manning, M. C.; Holcomb, R. E.; Payne, R. W.; Stillahn, J. M.; Connolly, B. D.; Katayama, D. S.; Liu, H.; Matsuura, J. E.; Murphy, B. M.; Henry, C. S.; et al. Stability of Protein Pharmaceuticals: Recent advances. *Pharm. Res.* **2024**, *41*, 1301–1367.

(8) Rivas, G.; Minton, A. P. Macromolecular Crowding In Vitro, In Vivo, and In Between. *Trends Biochem. Sci.* **2016**, *41*, 970–981.

(9) Inomata, K.; Ohno, A.; Tochio, H.; Isogai, S.; Tenno, T.; Nakase, I.; Takeuchi, T.; Futaki, S.; Ito, Y.; Hiroaki, H.; Shirakawa, M. High-resolution multi-dimensional NMR spectroscopy of proteins in human cells. *Nature* **2009**, *458*, 106–109.

(10) Miklos, A. C.; Sarkar, M.; Wang, Y.; Pielak, G. J. Protein Crowding Tunes Protein Stability. *J. Am. Chem. Soc.* **2011**, *133*, 7116–7120.

(11) Gnutt, D.; Gao, M.; Brylski, O.; Heyden, M.; Ebbinghaus, S. Excluded-Volume Effects in Living Cells. *Angew. Chem. Int. Ed.* **2015**, *54*, 2548–2551.

(12) van den Berg, J.; Boersma, A. J.; Poolman, B. Microorganisms maintain crowding homeostasis. *Nat. Rev. Microbiol.* **2017**, *15*, 309–318.

(13) Hartl, J.; Friesen, S.; Johannsmann, D.; Buchner, R.; Hinderberger, D.; Blech, M.; Garidel, P. Dipolar Interactions and Protein Hydration in Highly Concentrated Antibody Formulations. *Mol. Pharm.* **2022**, *19*, 494–507.

(14) Crescioli, S.; Kaplon, H.; Wang, L.; Visweswaraiah, J.; Kapoor, V.; Reichert, J. M. Antibodies to watch in 2025. *mAbs* **2025**, *17*, 2443538.

(15) Mathias, N. et al. Towards more tolerable subcutaneous administration: Review of contributing factors for improving combination product design. *Adv. Drug Deliv. Rev.* **2024**, *209*, 115301.

(16) Hermeling, S.; Crommelin, D. J. A.; Schellekens, H.; Jiskoot, W. Structure-Immunogenicity Relationships of Therapeutic Proteins. *Pharm. Res.* **2004**, *21*, 897–903.

(17) Hofmann, M.; Gieseler, H. Predictive Screening Tools Used in High-Concentration Protein Formulation Development. *J. Pharm. Sci.* **2018**, *107*, 772–777.

(18) Mieczkowski, C. A. The Evolution of Commercial Antibody Formulations. *J. Pharm. Sci.* **2023**, *112*, 1801–1810.

(19) Park, T.; Griggs, S. K.; Suh, D.-C. Cost effectiveness of monoclonal antibody therapy for rare diseases: A systematic review. *BioDrugs* **2015**, *29*, 259–274.

(20) Prass, T. M.; Garidel, P.; Blech, M.; Schäfer, L. V. Viscosity Prediction of High-Concentration Antibody Solutions with Atomistic Simulations. *J. Chem. Inf. Model.* **2023**, *63*, 6129–6140.

(21) Ladd, A. J. C. Hydrodynamic transport coefficients of random dispersions of hard spheres. *J. Chem. Phys.* **1990**, *93*, 3484–3494.

(22) Cichocki, B.; Felderhof, B. U. Diffusion coefficients and effective viscosity of suspensions of sticky hard spheres with hydrodynamic interactions. *J. Chem. Phys.* **1990**, *93*, 4427–4432.

(23) Virk, S. S.; Underhill, P. T. Application of a Simple Short-Range Attraction and Long-Range Repulsion Colloidal Model toward Predicting the Viscosity of Protein Solutions. *Mol. Pharm.* **2022**, *19*, 4233–4240.

(24) Chaudhri, A.; Zarraga, I. E.; Kamerzell, T. J.; Brandt, J. P.; Patapoff, T. W.; Shire, S. J.; Voth, G. A. Coarse-Grained Modeling of the Self-Association of Therapeutic Monoclonal Antibodies. *J. Phys. Chem. B* **2012**, *116*, 8045–8057.

(25) Buck, P. M.; Chaudhri, A.; Kumar, S.; Singh, S. K. Highly Viscous Antibody Solutions Are a Consequence of Network Formation Caused by Domain-Domain Electrostatic Complementarities: Insights from Coarse-Grained Simulations. *Mol. Pharm.* **2015**, *12*, 127–139.

(26) Chowdhury, A.; Bollinger, J. A.; Dear, B. J.; Cheung, J. K.; Johnston, K. P.; Truskett, T. M. Coarse-Grained Molecular Dynamics Simulations for Understanding the Impact of Short-Range Anisotropic Attractions on Structure and Viscosity of Concentrated Monoclonal Antibody Solutions. *Mol. Pharm.* **2020**, *17*, 1748–1756.

(27) Shahfar, H.; Forder, J. K.; Roberts, C. J. Toward a Suite of Coarse-Grained Models for Molecular Simulation of Monoclonal Antibodies and Therapeutic Proteins. *J. Phys. Chem. B* **2021**, *125*, 3574–3588.

(28) Ren, S. Effects of arginine in therapeutic protein formulations: a decade review and perspectives. *Antib. Ther.* **2023**, *6*, 265–276.

(29) Zhang, J.; Frey, V.; Corcoran, M.; Enk, J. Z.-V.; Subramony, J. A. Influence of Arginine Salts on the Thermal Stability and Aggregation Kinetics of Monoclonal Antibody: Dominant Role of Anions. *Mol. Pharm.* **2016**, *13*, 3362–3369.

(30) Maity, H.; O'Dell, C.; Srivastava, A.; Goldstein, J. Effects of Arginine on Photostability and Thermal Stability of IgG1 Monoclonal Antibodies. *Curr. Pharm. Biotechnol.* **2009**, *10*, 761–766.

(31) Tilegenova, C.; Izadi, S.; Yin, J.; Huang, C. S.; Wu, J.; Ellerman, D.; Hymowitz, S. G.; Walters, B.; Salisbury, C.; Carter, P. J. Dissecting the molecular basis of high viscosity of monospecific and bispecific IgG antibodies. *mAbs* **2020**, *12*, 1692764.

(32) Cloutier, T. K.; Sudrik, C.; Mody, N.; Hasige, S. A.; Trout, B. L. Molecular computations of preferential interactions of proline, arginine.HCl, and NaCl with IgG1 antibodies and their impact on aggregation and viscosity. *mAbs* **2020**, *12*, 1816312.

(33) Prass, T. M.; Garidel, P.; Schäfer, L. V.; Blech, M. Residue-resolved insights into the stabilization of therapeutic proteins by excipients: A case study of two monoclonal antibodies with arginine and glutamate. *mAbs* **2024**, *16*, 2427771.

(34) Lui, L.; Vanderwalle, C.; Brocchini, S.; Velayudhan, A. Discovering Novel Small Molecule Compound for Prevention of Monoclonal Antibody Self-Association. *Antibodies* **2022**, *11*, 40.

(35) King, T. E.; Humphrey, J. R.; Laughton, C. A.; Thomas, N. R.; Hirst, J. D. Optimizing Excipient Properties to Prevent Aggregation in Biopharmaceutical Formulations. *J. Chem. Inf. Model.* **2024**, *64*, 265–275.

(36) de Jong, D. H.; Singh, G.; Bennett, W. F. D.; Arnarez, C.; Wassenaar, T. A.; Schäfer, L. V.; Periole, X.; Tieleman, D. P.; Marrink, S. J. Improved parameters for the Martini coarse-grained protein force field. *J. Chem. Theory Comput.* **2013**, *9*, 687–697.

(37) Souza, P. C. T. et al. Martini 3: a general purpose force field for coarse-grained molecular dynamics. *Nat. Methods* **2021**, *18*, 382–388.

(38) Marrink, S. J.; Monticelli, L.; Melo, M. N.; Alessandri, R.; Tieleman, D. P.; Souza, P. C. T. Two decades of Martini: Better beads, broader scope. *Wiley Interdiscip. Rev. Comput. Mol. Sci.* **2023**, *13*, e1620.

(39) Borges-Araújo, L.; Pereira, G. P.; Valério, M.; Souza, P. C. T. Assessing the Martini 3 protein model: A review of its path and potential. *Biochim. Biophys. Acta - Proteins Proteom.* **2024**, *1872*, 141014.

(40) Thomasen, F. E.; Pesce, F.; Roesgaard, M. A.; Tesei, G.; Lindorff-Larsen, K. Improving Martini 3 for Disordered and Multidomain Proteins. *J. Chem. Theory Comput.* **2022**, *18*, 2033–2041.

(41) Thomasen, F. E.; Skaalum, T.; Kumar, A.; Srinivasan, S.; Vanni, S.; Lindorff-Larsen, K. Rescaling protein-protein interactions improves Martini 3 for flexible proteins in solution. *Nat. Commun.* **2024**, *15*, 6645.

(42) Binder, J.; Zalar, M.; Huelsmeyer, M.; Siedler, M.; Curtis, R.; Friess, W. Enhancing Martini 3 for protein self-interaction simulations. *Eur. J. Pharm. Sci.* **2025**, *209*, 107068.

(43) Wang, L.; Brasnett, C.; Borges-Araújo, L.; Souza, P. C. T.; Marrink, S. J. Martini3-IDP: Improved Martini 3 force field for disordered proteins. *Nat. Commun.* **2025**, *16*, 2874.

(44) Pedersen, K. B.; Borges-Araújo, L.; Stange, A. D.; Souza, P. C. T.; Marrink, S. J.; Schiøtt, B. OLIVES: A Gō-like Model for Stabilizing Protein Structure via Hydrogen Bonding Native Contacts in the Martini 3 Coarse-Grained Force Field. *J. Chem. Theory Comput.* **2024**, *20*, 8049–8070.

(45) Lamprakis, C.; Andreadelis, I.; Manchester, J.; Velez-Vega, C.; Duca, J. S.; Cournia, Z. Evaluating the Efficiency of the Martini Force Field to Study Protein Dimerization in Aqueous and Membrane Environments. *J. Chem. Theory Comput.* **2021**, *17*, 3088–3102.

(46) Zwanzig, R. Time-Correlation Functions and Transport Coefficients in Statistical Mechanics. *Annu. Rev. Phys. Chem.* **1965**, *16*, 67–102.

(47) Hess, B. Determining the shear viscosity of model liquids from molecular dynamics simulations. *J. Chem. Phys.* **2002**, *116*, 209–217.

(48) von Bülow, S.; Siggel, M.; Linke, M.; Hummer, G. Dynamic cluster formation determines viscosity and diffusion in dense protein solutions. *Proc. Natl. Acad. Sci. U.S.A.* **2019**, *116*, 9843–9852.

(49) Grünewald, F.; Punt, M. H.; Jefferys, E. E.; Vainikka, P. A.; König, M.; Virtanen, V.; Meyer, T. A.; Pezeshkian, W.; Gormley, A. J.; Karonen, M.; Sansom, M. S. P.; Souza, P. C. T.; Marrink, S. J. Martini 3 Coarse-Grained Force Field for Carbohydrates. *J. Chem. Theory Comput.* **2022**, *18*, 7555–7569.

(50) Lutsyk, V.; Wolski, P.; Plazinski, W. Extending the Martini 3 Coarse-Grained Force Field to Carbohydrates. *J. Chem. Theory Comput.* **2022**, *18*, 5089–5107.

(51) Brandner, A. F.; Smith, I. P. S.; Marrink, S. J.; Souza, P. C. T.; Khalid, S. Systematic Approach to Parametrization of Disaccharides for the Martini 3 Coarse-Grained Force Field. *J. Chem. Inf. Model.* **2025**, *65*, 1537–1548.

(52) Prass, T. M.; Lindorff-Larsen, K.; Garidel, P.; Blech, M.; Schäfer, L. V. Optimized Protein–Excipient Interactions in the Martini 3 Force Field. *J. Chem. Inf. Model.* **2025**, *65*, 3581–3592.

(53) Heisler, J.; Kovner, D.; Izadi, S.; Zarzar, J.; Carter, P. J. Modulation of the high concentration viscosity of IgG1 antibodies using clinically validated Fc mutations. *mAbs* **2024**, *16*, 2379560.

(54) Tsumura, K.; Hsu, W.; Mimura, M.; Horiuchi, A.; Shiraki, K. Lowering the viscosity of a high-concentration antibody solution by protein–polyelectrolyte complex. *J. Biosci. Bioeng.* **2022**, *133*, 17–24.

(55) Ross, P. D.; Minton, A. P. Hard quasispherical model for the viscosity of hemoglobin solutions. *Biochem. Biophys. Res. Commun.* **1977**, *76*, 971–976.

(56) Ostrowska, N.; Feig, M.; Trylska, J. Modeling Crowded Environment in Molecular Simulations. *Front. Mol. Biosci.* **2019**, *6*, 86.

(57) Stevens, J. A.; Grünewald, F.; van Tilburg, P. A. M.; König, M.; Gilbert, B. R.; Brier, T. A.; Thornburg, Z. R.; Luthey-Schulten, Z.; Marrink, S. J. Molecular dynamics simulation of an entire cell. *Front. Chem.* **2023**, *11*, 1106495.

(58) Wright, J. D.; Chu, H. M.; Huang, C. H.; Ma, C.; Chang, T. W.; Lim, C. Structural and Physical Basis for Anti-IgE Therapy. *Sci. Rep.* **2015**, *5*, 11581.

(59) Martí-Renom, M. A.; Stuart, A. C.; Fiser, A.; Sánchez, R.; Melo, F.; Šali, A. Comparative Protein Structure Modeling of Genes and Genomes. *Annual Review of Biophysics* **2000**, *29*, 291–325.

(60) Fiser, A.; Do, R. K. G.; Šali, A. Modeling of loops in protein structures. *Prot. Sci.* **2000**, *9*, 1753–1773.

(61) Brandt, J. P.; Patapoff, T. W.; Aragon, S. R. Construction, MD simulation, and hydrodynamic validation of an all-atom model of a monoclonal IGG antibody. *Biophys. J.* **2010**, *99*, 905–913.

(62) Kroon, P. C.; Grünewald, F.; Barnoud, J.; van Tilburg, M.; Souza, P. C. T.; Wassenaar, T. A.; Marrink, S. J. Martinize2 and Vermouth: Unified Framework for Topology Generation. *eLife* **2023**, *12*, RP90627.

(63) Herzog, F. A.; Braun, L.; Schoen, I.; Vogel, V. Improved Side Chain Dynamics in MARTINI Simulations of Protein–Lipid Interfaces. *J. Chem. Theory Comput.* **2016**, *12*, 2446–2458.

(64) Abraham, M. J.; Murtola, T.; Schulz, R.; Páll, S.; Smith, J. C.; Hess, B.; Lindahl, E. GROMACS: High performance molecular simulations through multi-level parallelism from laptops to supercomputers. *SoftwareX* **2015**, *1-2*, 19–25.

(65) Bussi, G.; Donadio, D.; Parrinello, M. Canonical sampling through velocity rescaling. *J. Chem. Phys.* **2007**, *126*, 014101.

(66) Bernetti, M.; Bussi, G. Pressure control using stochastic cell rescaling. *J. Chem. Phys.* **2020**, *153*, 114107.

(67) de Jong, D. H.; Baoukina, S.; Ingólfsson, H. I.; Marrink, S. J. Martini straight: Boosting performance using a shorter cutoff and GPUs. *Comput. Phys. Commun.* **2016**, *199*, 1–7.

(68) Kim, H.; Fábián, B.; Hummer, G. Neighbor List Artifacts in Molecular Dynamics Simulations. *J. Chem. Theory Comput.* **2023**, *19*, 8919–8929.

(69) Rey-Castro, C.; Vega, L. F. Transport Properties of the Ionic Liquid 1-Ethyl-3-Methylimidazolium Chloride from Equilibrium Molecular Dynamics Simulation. The Effect of Temperature. *J. Phys. Chem. B* **2006**, *110*, 14426–14435.

(70) Holian, B. L.; Evans, D. J. Shear viscosities away from the melting line: A comparison of equilibrium and nonequilibrium molecular dynamics. *J. Chem. Phys.* **1983**, *78*, 5147–5150.